Atomic layer deposition of TbF_3 thin films

Running title: Atomic layer deposition of TbF_3 thin films
Running Authors: Atosuo et al.

Elisa Atosuo[a)], Juha Ojala, Mikko J. Heikkilä, and Miika Mattinen
Department of Chemistry, University of Helsinki, P.O. Box 55, FI-00014 Helsinki, Finland

Kenichiro Mizohata and Jyrki Räisänen
Department of Physics, University of Helsinki, P.O. Box 43, FI-00014 Helsinki, Finland

Markku Leskelä and Mikko Ritala
Department of Chemistry, University of Helsinki, P.O. Box 55, FI-00014 Helsinki, Finland

[a)] Electronic mail: elisa.atosuo@helsinki.fi

ABSTRACT

Lanthanide fluoride thin films have gained interest as materials for various optical applications, including electroluminescent displays and mid-IR lasers. The number of atomic layer deposition (ALD) processes for lanthanide fluorides has remained low, however. In this work, we present an ALD process for TbF_3 using tris(2,2,6,6-tetramethyl-3,5-heptanedionato)terbium ($Tb(thd)_3$) and TiF_4 as precursors. The films were grown at 175–350 °C. The process yields weakly crystalline films at the lowest deposition temperature, whereas strongly crystalline, orthorhombic TbF_3 films are obtained at higher temperatures. The films deposited at 275–350 °C are exceptionally pure, with low contents of C, O, and H, and the content of titanium is below the detection limit (<0.1 at-%) of time-of-flight elastic recoil detection analysis (ToF-ERDA). Due to the lack of titanium impurities, the films show high transmittance down to short UV wavelengths.

I. INTRODUCTION

Owing to their exceptional luminescence properties, lanthanide fluoride thin films have gained interest as materials for various optical applications, including electroluminescent displays and mid-IR lasers. The unique properties of lanthanide fluorides stem from the electronic structure of the cations as well as the host properties of fluorides. In lanthanide ions, the 4f electrons responsible for the luminescence are well shielded by the electrons in outer orbitals, leading to low coupling with matrix phonons and therefore to sharp transitions upon excitation and de-excitation. Metal fluorides, due to their low phonon energies, offer less pathways for non-radiative relaxation and serve therefore as excellent host materials for luminescence centers.[1, 2] Lanthanide fluorides have become essential parts of applications utilizing either electroluminescence or photoluminescence, such as TbF_3 in green-light emitting $ZnS:TbF_x$ in electroluminescent displays[3] and NdF_3 in mid-IR lasers[4]. Moreover, when combined with each other, lanthanide fluorides have shown to be applicable for white-light emission in solid-state lighting applications.[5–7]

Other technologically important properties arise from the large electronegativity difference of fluorine and lanthanides. The resulting ionic character of the bonds leads to high band gaps (>7 eV) and low refractive indices. The high band gap is essential for optical applications at short-wavelength UV range whereas the low refractive index is exploited in multilayer interference coatings. A wide selection of lanthanide fluorides, for instance LaF_3, CeF_3, PrF_3, and GdF_3, have gained interest as antireflective coatings.[8–11] The insulating nature of metal fluorides, in turn,

has sparked up the research on capacitor applications. For EuF_3, a dielectric constant around 11 has been reported[12], and for SmF_3 the dielectric constants have been around 9 and 11.[Refs. 13–14]

In addition to the aforementioned binary lanthanide fluorides, many new possibilities emerge when lanthanide fluorides are combined with other metal fluorides, for example those of alkali metals. Currently, $NaGdF_4$ is among the most promising host materials for upconversion luminescence applications[15], whereas KTb_3F_{10} has been shown to exhibit excellent magneto-optical properties.[16] As a solid-state laser host material, for example $LiLuF_4$ has attracted wide attention.[17]

Given the selection of applications for lanthanide fluoride thin films, surprisingly many lack an atomic layer deposition (ALD) process. For the synthesis of lanthanide fluoride thin films, mostly physical vapor deposition (PVD) methods have been used. Although PVD methods are suitable for depositing films on flat surfaces, the film quality deteriorates remarkably when the surface features become more complex and shrink in size. ALD, in turn, is a chemical deposition method known for its capability of producing conformal films also on complicated structures, namely high aspect-ratio substrates and nanoparticles. ALD is based on self-limiting surface reactions of alternatively supplied gaseous precursors, which enables uniform film deposition, precise thickness control and excellent reproducibility. Yet one of the peculiar features of ALD is the ability to deposit submonolayers of materials in a controllable manner, which is beneficial in systems where uniform distribution of dopants is desired, for example in luminescence devices. Consequently, ALD is today considered as the state-of-the-art thin film deposition method in numerous fields.[18]

The main reason for the limited number of ALD processes for lanthanide fluorides lies, on one hand, in the hazardousness and toxicity of the most efficient fluoride source, hydrogen fluoride. Even though HF has sometimes been formed inside the reactor by decomposing NH_4F [Ref. 19] — which diminishes the exposure risk of the operator — HF can still damage the glass and metal parts inside the reactor. On the other hand, the use of relatively safe alternatives to HF, for example TiF_4 and TaF_5, often results in some metal impurities in the films.[20–26] Metal impurities increase absorption in the UV wavelengths, and are thus detrimental for optical applications. For many years, of the rare earth fluorides only LaF_3 and YF_3 ALD processes were found in the literature.[22, 24] While writing this article, deposition of SmF_3, EuF_3, and TbF_3 was presented as a part of an organic–inorganic laminate deposition process[27].

In this paper, we present an ALD process for terbium(III) fluoride films using $Tb(thd)_3$ and TiF_4 as precursors. The most important outcome of this study is that, unlike in many previous TiF_4-based processes, TbF_3 can be deposited without titanium incorporation into the films. The lack of titanium impurities, together with the general properties of lanthanide fluorides, can make ALD-TbF_3 a suitable material for antireflection applications, for example.

II. EXPERIMENTAL

A. Film deposition

The films were deposited using an F120 cross-flow ALD reactor (ASM Microchemistry Ltd.) at a pressure of approximately 10 mbar. N_2 (99.999%) was used as a carrier and purging gas. $Tb(thd)_3$ (Volatec Oy, Finland) and TiF_4 (Strem Chemicals Inc., 98%) were used as precursors. Both precursors were evaporated from glass boats inside the reactor at 135–138 °C. The deposition temperature was varied between 175 and 350 °C. Most of the depositions were done on 5 cm x 5 cm Si(100) substrates with the native oxide. For UV–Vis transmission measurements, some films were deposited on 2'', double-side polished, c-plane (0001) sapphire substrates (University wafers).

B. Film characterization

Film thicknesses and refractive indices were measured using a Film Sense FS-1 Multi-wavelength ellipsometer. Cauchy model was used to fit the data. To confirm the thicknesses, some samples were measured also with x-ray reflectivity (XRR) using a PANalytical X'pert Pro MPD diffractometer. The density of the films was determined from the XRR curves. The same instrument in the x-ray diffraction (XRD) mode was used for determining the crystallinity and crystalline phases. For phase identification, HighScore plus software (version 4.7) from PANalytical was used.

Morphology of the films was studied with a Hitachi S-4800 field-emission scanning electron microscope (FESEM). Due to the insulating nature of the films, the samples were coated with Au/Pd alloy before the measurement. Atomic force microscope (AFM) images were recorded using a Veeco Multimode V instrument for analyzing

surface roughness and morphology. Tapping mode images were captured in air using silicon probes with a nominal tip radius of 10 nm and a nominal spring constant of 3 N/m (NFESP from Bruker). Images were flattened to remove artefacts caused by sample tilt and scanner bow. Roughness was calculated as a root-mean-square value (R_q).

For elemental composition analysis, energy dispersive x-ray spectroscopy (EDS) measurements were done with an Oxford INCA 350 microanalysis system connected to the FESEM instrument. Prior to measuring, samples were coated with a thin Au/Pd alloy layer. For quantitative studies on stoichiometry and impurities, time-of-flight elastic recoil detection analyses (ToF-ERDA) were conducted with a 5 MV tandem accelerator EGP-10-II using 40 MeV $^{79}Br^{7+}$ ions with a detection angle of 40°. To evaluate the transmission properties of the films, UV–Vis transmission spectra were measured by a Hitachi U2000 spectrophotometer in a wavelength range of 190–1100 nm. Film adhesion to the substrate was tested with the Scotch tape test.

III. RESULTS AND DISCUSSION

A. Film growth

The self-limiting film growth mode of the process was verified at 300 °C. The saturation of the growth rate with respect of the $Tb(thd)_3$ pulse was studied by varying the pulse duration between 0.5 and 5 s while keeping the TiF_4 pulse at 1 s and purges at 2 s. As seen in Fig. 1(a) (black squares), saturation is achieved with 3 s pulses, resulting in a growth rate of 0.75 Å/cycle. However, a slight increase in the growth rate is seen for 5 s pulses.

The effect of purging time on the growth rate was studied by varying the purge time for both of the precursors simultaneously. Purge lengths of 2 to 6 s were applied

while keeping the $Tb(thd)_3$ pulse at 5 s and the TiF_4 pulse at 1 s. Fig. 1(b) shows a small but clear decrease in the growth rate between 2 s and 4 s purges, after which the growth rate saturates to 0.68 Å/cycle. In Fig. 1(a), red triangles depict the effect of the $Tb(thd)_3$ pulse length on the growth rate with 4 s purges. As can be seen from Fig. 1(a), also in this case 3 s pulse is sufficient for $Tb(thd)_3$.

The saturation behavior of the TiF_4 pulse was tested by varying the pulse length between 0.2 and 2.0 s. The $Tb(thd)_3$ pulse was set as 3 s and both purges were 4 s. As seen in Fig. 1(c), the saturation of the growth rate is achieved with 1 s TiF_4 pulses. Thus, 3 s $Tb(thd)_3$ pulse, 1 s TiF_4 pulse and 4 s purges were applied in further depositions. It should be noted, that in this process the purge time needed to remove excess molecules from the reaction surface is relatively long for an F120 ALD reactor, especially when considering the high deposition temperature.

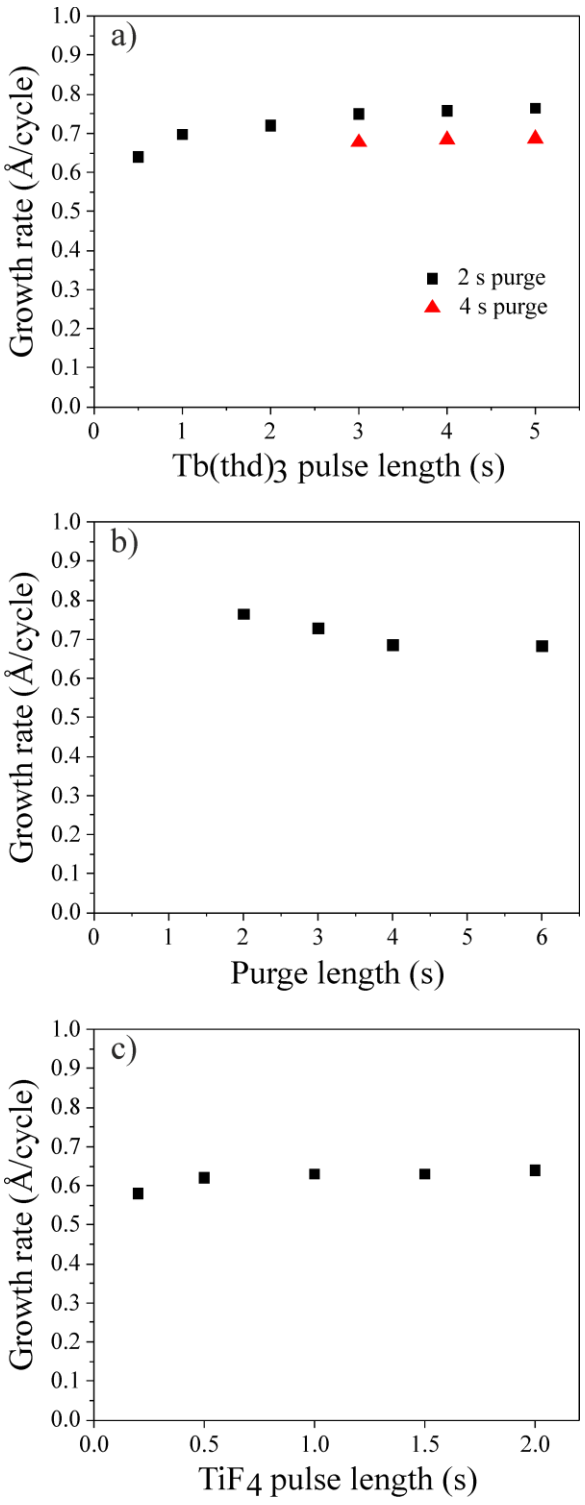

FIG. 1. Growth rate versus a) $Tb(thd)_3$ pulse length with 2 and 4 s purges, b) purge length, and c) TiF_4 pulse length.

The thickness of the films versus the number of cycles was investigated at 300 °C. The film thickness grows almost linearly, increasing from 270 Å for a 400 cycle film to 1000 Å for a 1500 cycle film as illustrated in Fig. 2.

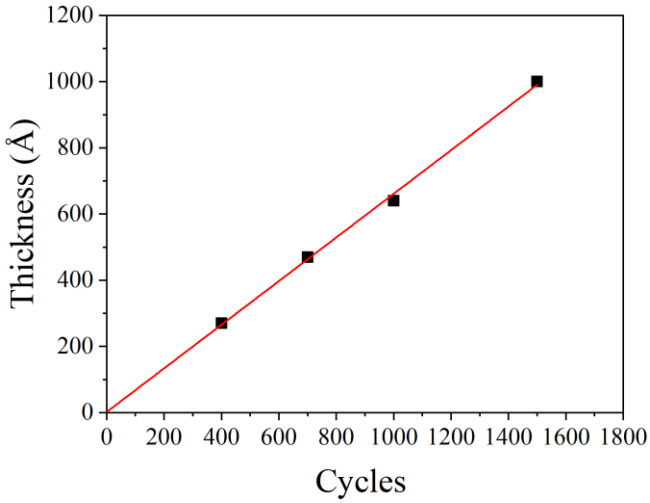

FIG. 2. Film thickness as a function of cycle number at deposition temperature of 300 °C.

The dependence of the growth rate on the temperature was investigated by varying the deposition temperature from 175 to 350 °C while keeping the pulse and purge lengths constant. The pulse durations were obtained from the saturation tests at 300 °C and may not fall in the saturation regimes at all the other temperatures. Therefore, the growth rates should be regarded as tentative. The growth rate is strongly dependent on the deposition temperature (Fig. 3). At the lowest temperature, the growth rate has the maximum value of 1.45 Å/cycle. At higher temperatures, the growth rate decreases almost linearly, until at 275 °C a deviation from this trend occurs. At higher temperatures, the growth rate seems to follow the original trend, resulting in a growth rate

of 0.45 Å/cycle at the highest studied temperature (350 °C). The decreasing trend of the growth rate may be associated with decreasing density of TiF_x groups on the surface. Similar trends of decreasing growth rates have been observed in previous studies using TiF_4 as a precursor, and also the role of TiF_x surface groups has been proposed earlier.[20–22, 24, 25, 28] In general, however, the growth rates are low compared to the other ALD metal fluoride processes using thd precursors and TiF_4. The growth rates in these processes at 300 °C, for example, are typically 1.2–1.6 Å/cycle.[20, 21, 24, 28] For the extreme case of LaF_3, the growth rate is as high as 5.2 Å/cycle at 225–250 °C.[22] To explain the unusually high growth rates, an uncommon growth mechanism was proposed: instead of forming only after a complete ALD cycle, LaF_3 is formed in each half cycle. During the $La(thd)_3$ pulse, the ligand exchange reactions occur as usual, but also an additional layer of $La(thd)_3$ molecules adsorbs onto the deposited LaF_3 surface. Similar additional layer adsorbs also during the TiF_4 pulse. Judging from the growth rate of TbF_3 it is likely that the film growth does not proceed in a similar manner. A more detailed study would be required to confirm the growth mechanism, however.

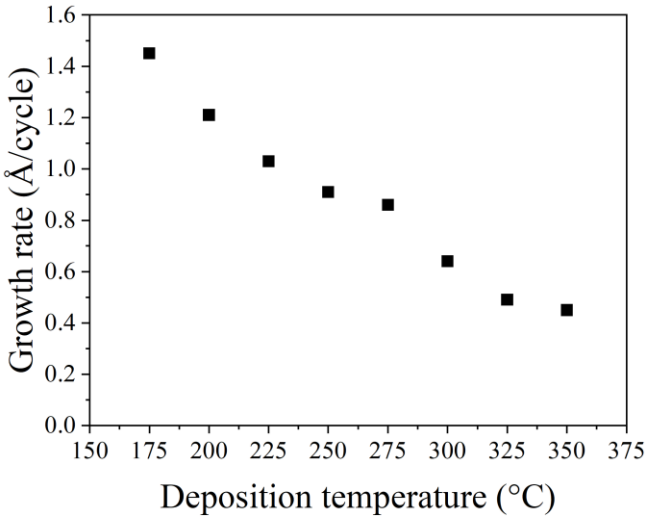

FIG. 3. Growth rate as a function of deposition temperature. Pulse length for $Tb(thd)_3$ was 3 s and for TiF_4 1 s. Purge time was 4 s for both of the precursors.

B. Film properties

To determine and compare the crystal structure of the films deposited at different temperatures, grazing incidence (GI) XRD measurements were conducted. Figs. 4(a) and 4(b) depict the x-ray diffractograms for approximately 100 nm films deposited at 175–350 °C. As seen in Fig. 4(a), the lowest deposition temperature yields weakly crystalline films and only one reflection at a 2θ angle of ~25.5° is present.

The crystallinity increases in the samples deposited at 200–250 °C, as several new reflections emerge. The reflections coincide well with the reference pattern of the orthorhombic TbF_3[Ref. 29], except for an additional reflection observed at a 2θ angle of ~29°. The origin of this reflection could not be identified, but it coincides well with the characteristic reflection of the cubic rare earth oxides at a 2θ angle of ~29°.[Ref.30] For the cubic Tb_2O_3, the reflection is observed at a 2θ angle of 28.8°.[Ref. 31] The next notable change in the crystal structure occurs at 275 °C, when the additional reflection at ~29°

disappears [Fig. 4(b)]. No further changes are seen when the deposition temperature is increased from 275 to 350 °C, but interestingly the strongest reflections in the temperature series are measured from the film deposited at 275 °C.

The relative intensities of the reflections measured from the films deposited at 250–300 °C differ from the other films. The (210) reflection at 30.3° is pronounced, especially in the 275 °C sample. For all the other deposition temperatures, the strongest reflections are obtained at 2θ angles of 27.6° (111) and 30.3° (210), which is more in line with the relative intensities of the TbF_3 reference pattern. To determine the orientation of the films, 2θ–ω measurements were conducted. Fig. 5 illustrates the results for the films deposited at 275 and 350 °C. To eliminate the reflections from the silicon substrate, the omega offset was set to 4°. As depicted in Fig. 5, at 275 °C the reflection originating from the (210) planes at a 2θ angle of 30.3° is pronounced. For the majority of the crystallites, the (210) planes are thus nearly parallel to the surface. For a film deposited at 350 °C, the reflections at 25.6° (020) and 52.7° (040) are missing, indicating a preferred orientation also at this deposition temperature. The details of the orientation were not investigated further, however.

The densities of the films were obtained from XRR curves. Due to the high roughness of the films, no clear oscillation was observed, but based on the critical angle the density of ~100 nm thick films deposited at 275, 300, and 350 °C isapproximately 7.0 g/cm^3. The bulk density of TbF_3 is 7.23 g/cm^3.[Ref. 32]

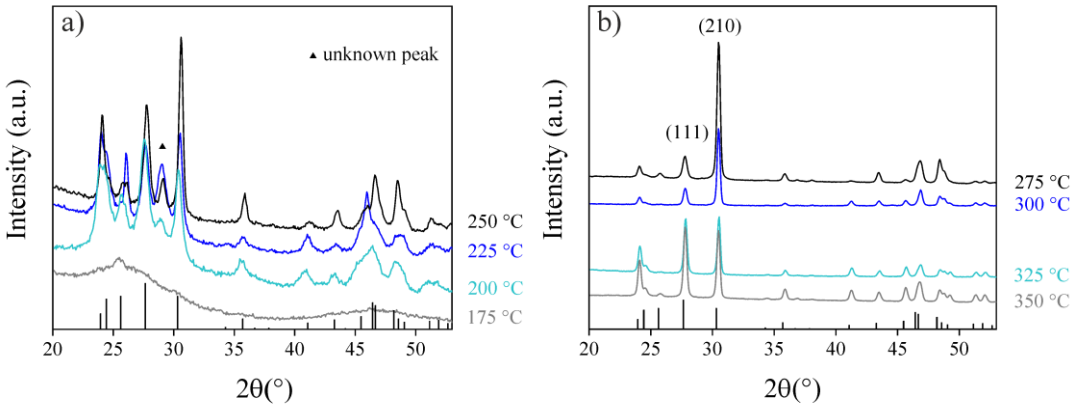

FIG. 4. Grazing incidence diffractograms of approximately 100 nm films deposited at a) 175–250 °C and b) 275–350 °C. The black columns depict the reference pattern of the orthorhombic TbF_3. In b) the relative intensities of the films deposited at 300 and 325 °C have been increased for easier comparison.

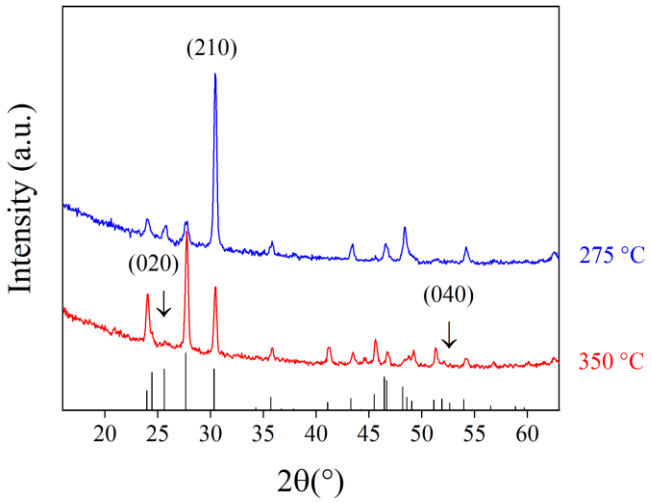

FIG. 5. 2θ–ω measurements for the films deposited at 275 and 350 °C and the reference pattern of TbF_3. The omega offset was set to 4° to eliminate the reflections from the silicon substrate.

For each deposition temperature, the composition of the film was determined qualitatively by EDS (results not shown here). For the films deposited at 250 °C and above, only Tb, F, C, and O were detected. In turn, the films deposited at 225 °C and

below showed traces of titanium. For quantitative determination of the impurities and stoichiometry of the films, selected samples were measured with ToF-ERDA.
Table I lists the measured stoichiometry ratios and impurities for approximately 100 nm thick films deposited at different temperatures. Based on the impurity levels, the films can be divided into two distinct groups and are therefore presented separately in the text. For the three lowest deposition temperatures up to 225 °C, modest impurity levels are detected. The content of H is the highest, increasing from 5.9 at-% for the 175 °C sample to 7.8 at-% for the 225 °C sample. The content of C is 4.3–5.3 at-%, being the highest for the 200 °C sample. Oxygen impurity levels vary between 4.5 and 5.6 at-%, decreasing as the deposition temperature is increased. Also titanium impurities were detected in these samples. The highest content, 3.7 at-%, is obtained for the film deposited at the lowest temperature. In addition, the films are fluorine rich. The F:Tb ratio for the lowest deposition temperature is 3.5, whereas for the films deposited at 200 and 225 °C it is 3.4. The films eroded during the measurement and therefore accurate depth profiles could not be obtained.

When the deposition temperature is increased to 275 °C and above, generally less than 1 at-% of C, O, and H is present in the films. Exceptions are the film deposited at 275 °C, where the oxygen content is larger (1.7 at-%), and the film deposited at 350 °C, where the hydrogen content is larger (1.0 at-%). Most importantly, the content of titanium is below the detection limit of ERDA, which would otherwise be 0.1 at.%, but because of sample erosion a more conservative estimate of 0.2 at.% could be made. The stoichiometry of the films also corresponds well to TbF_3, being 3.0, 2.9, and 3.0 for the 275, 300, and 350 °C samples, respectively.

TABLE I. Elemental composition and stoichiometry of approximately 100 nm films measured by ToF-ERDA.

Deposition temperature (°C)	Tb (at-%)	F (at-%)	H (at-%)	C (at-%)	O (at-%)	Ti (at-%)	F/Tb
175	17.8 ± 0.3	62.7 ± 1.2	5.9 ± 1.5	4.3 ± 0.3	5.6 ± 0.4	3.7 ± 0.2	3.5
200	18.3 ± 0.2	61.4 ± 0.8	7.2 ± 1.2	5.3 ± 0.2	5.1 ± 0.2	2.64 ± 0.13	3.4
225	18.5 ± 0.2	62.3 ± 0.7	7.8 ± 1.2	4.3 ± 0.2	4.5 ± 0.2	2.47 ± 0.12	3.4
275	24.32 ± 0.14	73.0 ± 1.0	0.8 ± 0.3	0.24 ± 0.04	1.68 ± 0.15		3.0
300	25.27 ± 0.15	72.7 ± 1.0	0.3 ± 0.2	0.9 ± 0.2	0.89 ± 0.11		2.9
350	24.36 ± 0.15	73.0 ± 1.1	1.0 ± 0.7	0.93 ± 0.14	0.72 ± 0.08		3.0

The absence of titanium in the films is uncommon for the TiF_4-based ALD fluoride processes, and only the LiF processes resulted in titanium free films at modest deposition temperatures.[28, 33] To estimate the feasibility of the ligand exchange reaction, thermodynamics were calculated for the formation of TbF_3 as well as for the previously published ALD metal fluorides. The calculations were done with HSC Chemistry 5.11 software (Outokumpu Research Oy) in bulk form using e.g. a reaction $2\ Tb_2O_3 + 3\ TiF_4 \rightarrow 4\ TbF_3 + 3\ TiO_2$. In absence of thermodynamic data for the metal-thd complexes, corresponding oxides had to be used as an approximation for the metal – oxygen bonds in all of the studied processes. Table II lists the calculated Gibbs free energies for the formation of one mole of metal fluorides at 300 °C. The Gibbs free energy for the formation of bulk TbF_3 does not stand out from the other materials; both lower and higher ΔG values are obtained for the previously published ALD metal fluoride processes. Thermodynamics is therefore unlikely the reason for the different behavior of the TbF_3 process.

TABLE II. Calculated Gibbs free energies in kJ/mol for the formation of 1 mol of metal fluorides at 300 °C.

Material	Calculated ΔG (kJ/mol)
LaF_3	-261
CaF_2	-234
TbF_3	-231
YF_3	-230
MgF_2	-163
LiF	-139

However, as stated earlier, we assume the TbF_3 growth to proceed in a different manner compared to the previous TiF_4-based processes. The more conventional reaction mechanism of TbF_3 could partly explain the purity of the films. As no adsorption of an additional precursor layer appears to be involved, the shielding effect of the adsorbates is absent, and thus the ligand exchange reactions are more likely to be completed. Providing the deposition temperature is sufficient, films with titanium content less than 0.1 at-% (detection limit of ToF-ERDA) are obtained.

The morphology of the films was studied with FESEM. Fig. 6 shows FESEM images of approximately 100 nm thick films deposited at selected temperatures between 175 and 350 °C. At the lowest temperature, the surface of the film is relatively featureless. This is in accordance with XRD, which showed the film to be only weakly

crystalline. Upon increasing the deposition temperature to 200 °C and further, more features appear on the surface and the grains grow in size. A deviation from this trend is seen at 275 °C, where more sharp-edged grains are seen. The different morphology could be explained by the different texture of the sample as observed in the XRD measurements.

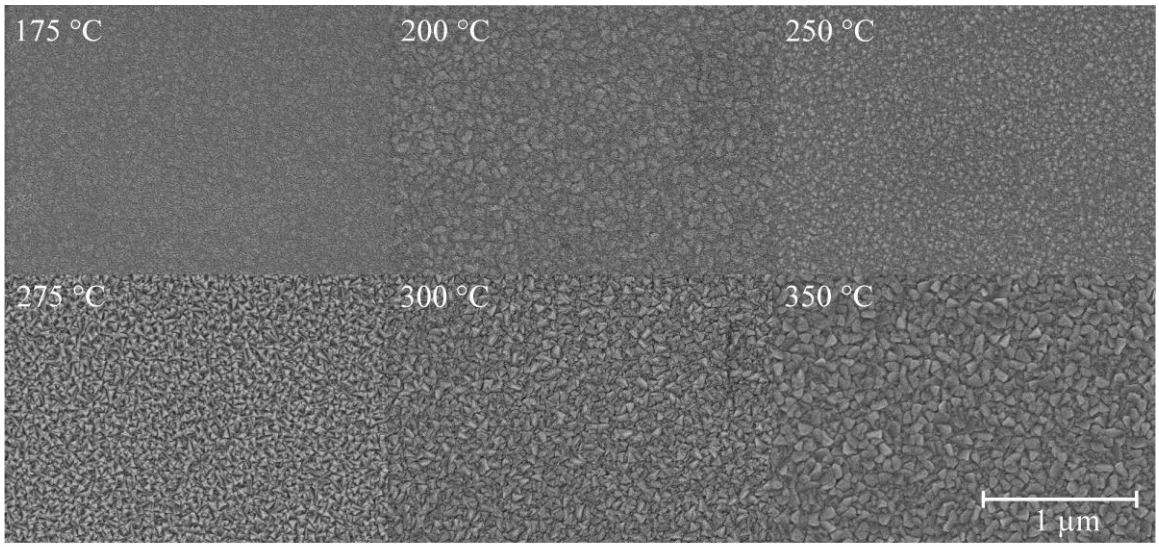

FIG. 6. FESEM images of approximately 100 nm thick films deposited at 175–350 °C.

To investigate the morphology of the films further, samples deposited at 275, 300, and 350 °C were measured with AFM. The 300 and 350 °C samples represent the films where titanium was not detected whereas the 275 °C sample was chosen for further investigation due to the anomaly observed in the earlier characterization steps. Figs. 7(a)–7(c) show AFM images of approximately 100 nm thick films and the calculated roughness as a root-mean-square value (R_q). As expected, the roughness of the film deposited as 275 °C is remarkable (R_q 8.6 nm) and exceeds the R_q value of the film deposited at 300 °C (5.6 nm). The largest R_q value, 9.8 nm, is however obtained for the

film deposited at 350 °C. To investigate the effect of the film thickness on the roughness, a 150 nm thick film deposited at 300 °C was measured [Fig. 7(d)]. The roughness increases from 5.6 nm to 8.4 nm, but is still less than the roughness measured for the 100 nm thick film deposited at 275 °C. In a wider perspective, our process seems to yield slightly rougher films compared to the other TiF_4-based processes.[21, 22, 24] For LiF films larger roughness was reported, however.[28]

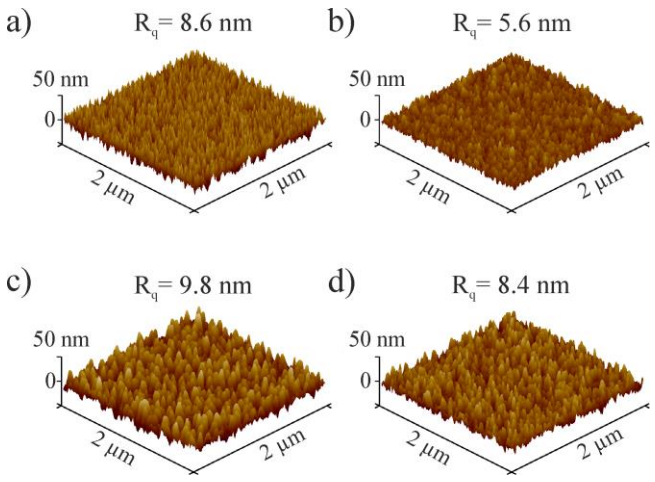

FIG. 7. AFM images and calculated R_q values of approximately 100 nm thick films deposited at a) 275 °C, b) 300 °C, c) 350 °C, and d) a 150 nm film deposited at 300 °C.

The refractive indices of the films were measured by ellipsometry. For the films deposited at 175–350 °C, the refractive index varies between 1.54 and 1.59 at 633 nm wavelength. For the bulk TbF_3, refractive index of 1.6034 has been reported (589 nm).[Ref. 34] It is well known that thin films tend to have lower refractive indices than the same materials in bulk form. However, evaluating the quality of the present TbF_3 films from the refractive indices is more complicated, especially at lower deposition

temperatures, as the lower density of the films decreases the refractive index whereas the oxide impurities increase the refractive index.

Due to the absence of titanium impurities in the films deposited at high temperatures, the absorbance of the films was predicted to be low across the whole UV–IR region of the electromagnetic spectrum. Fig. 8 depicts the transmittance spectra at 190–1100 nm wavelength range for a pristine sapphire substrate and a 37 nm TbF_3 film deposited on the sapphire substrate at 300 °C. As can be deduced from the figure, no additional absorbance occurs in the TbF_3/sapphire sample compared to the bare sapphire. The higher transmittance of the film compared to the bare substrate is explained by the higher refractive index of sapphire, being higher than 1.75 in the chosen wavelength range.[35] Therefore the TbF_3 film serves as an antireflection coating and increases the transmittance.

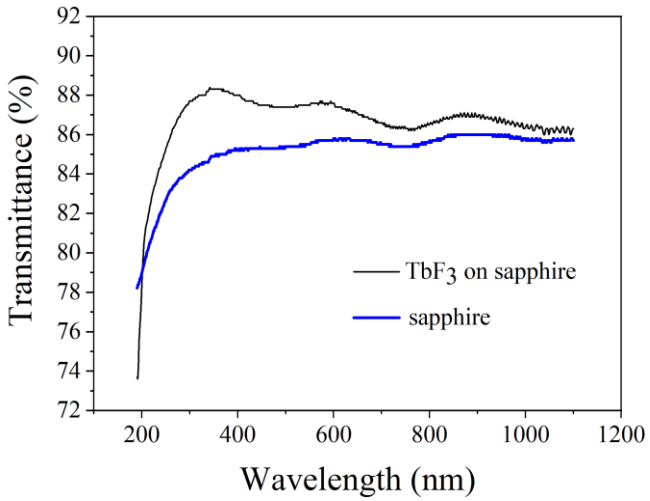

FIG. 8. UV–Vis transmission spectra measured for sapphire substrate (blue, bolded line) and TbF_3 film on sapphire.

Throughout the study, the films were stored at ambient conditions. After six months, no changes were seen in their visual appearance. According to XRD, no changes occurred in the crystal structure either. In addition to being stable in ambient air, all the films passed the Scotch tape test, indicating good adhesion to the silicon substrate.

IV. SUMMARY AND CONCLUSIONS

In this work, TbF_3 films were deposited by atomic layer deposition (ALD). The films were deposited at 175–350 °C using tris(2,2,6,6-tetramethyl-3,5-heptanedionato)terbium ($Tb(thd)_3$) and TiF_4 as precursors. The process obeys well the characteristics of ALD in terms of saturation of the growth rate with respect to precursor pulses and purges as tested at 300 °C. The thickness of the film also grows linearly with applied cycles. Similar to the other TiF_4-based ALD processes, the growth rate is strongly dependent on the deposition temperature, decreasing from 1.45 Å/cycle to 0.45 Å/cycle along the increasing deposition temperature. The lowest deposition temperature yields weakly crystalline films whereas at higher temperatures orthorhombic TbF_3 is obtained. The films deposited at 275 °C and above are stoichiometric and pure according to ToF-ERDA. Only small H, C, and O contents were detected in the films. Most importantly, and in contrast to most of the other TiF_4-based ALD metal fluoride processes, the content of titanium is below the detection limit of ToF-ERDA (<0.1 at-%). Due to the lack of titanium impurities, the films also show high transmittance at a wavelength range of 190–1100 nm. The films are stable in ambient air for at least several months, as no changes were seen in visual appearance and in XRD. In addition, all the films passed the Scotch tape test, indicating good adhesion to the silicon substrate.

As typical for metal fluoride films, the roughness of the film is remarkable, however, e.g. 5.6 nm for a 100 nm film deposited at 300 °C.

The data that support the findings of this study are available from the corresponding author upon reasonable request.

[1]J. Andres and A. Chauvin, *The Rare Earth Elements*, edited by David A. Atwood (Wiley, Chichester, 2012), pp. 111–133.

[2]R. K. Sharma, A. Mudring, and P. Ghosh, J. Lumin. **189**, 44 (2017).

[3]M. Leskelä and L. Niinistö, Mater. Chem. Phys. **31**, 7 (1992).

[4]J. Azkargorta, I. Iparraguirre, R. Balda, and J. Fernández, Opt. Express **16,** 11894 (2008).

[5]F. N. Sayed, V. Grover, K. A. Dubey, V. Sudarsan, and A. K. Tyagi, J. Colloid Interface Sci. **353**, 445 (2011).

[6]S. Sivakumar, F. C. J. M. van Veggel, and M. Raudsepp, J. Am. Chem. Soc. **127**, 12464 (2005).

[7]F. N. Sayed, V. Grover, S. V. Godbole, and A. K. Tyagi, RSC Adv. **2**, 1161 (2012).

[8]M. Bischoff, D. Gäbler, N. Kaiser, A. Chuvilin, U. Kaiser, and A. Tünnermann, Appl. Opt. **47**, C157 (2008)

[9]O. K. Simya, K. Balachander, D. Dhanalakshmi, and A. Ashok, Superlattice microst. **145**, 106579 (2020).

[10]B. Li, P. Xie, W. Su, X. Ma, H. Luo, and D. Liu, Mater. Des. **107**, 302 (2016).

[11]T. Yoshida, K. Nishimoto, K. Sekine, and K. Etoh, Appl. Opt. **45**, 1375 (2006).

[12]P. Meena, C. Balasubramanian, S. K. Narayandass, and D. Mangalaraj, Thin Solid Films **252**, 67 (1994).

[13]T. Mahalingam, M. Radhakrishnan, and C. Balasubramanian, Thin Solid Films **74**, 29 (1980).

[14]M. B. Shalimova and N. V. Sachuk, Semiconductors **53**, 229 (2019).

[15]F. Wang, R. Deng, J. Wang, Q. Wang, Y. Han, H. Zhu, X. Chen, and X. Liu, Nat. Mater. **10**, 968 (2011).

[16]D. Vojna, M. Duda, R. Yasuhara, O. Slezák, W. Schlichting, K. Stevens, H. Chen, A. Lucianetti, and T. Mocek, Opt. Lett. **45**, 1683 (2020).

[17]F. Cornacchia, A. Toncelli, and M. Tonelli, Prog. Quant. Electron. **33**, 61 (2009).

[18]M. Leskelä and M. Ritala, Angew. Chem. Int. Ed. **42**, 5548 (2003).

[19]M. Ylilammi and T. Ranta-aho, J. Electrochem. Soc. **141**, 1278 (1994).

[20]T. Pilvi, K. Arstila, M. Leskelä, and M. Ritala, Chem. Mater. **19**, 3387 (2007).

[21]T. Pilvi, T. Hatanpää, E. Puukilainen, K. Arstila, M. Bischoff, U. Kaiser, N. Kaiser, M. Leskelä, and M. Ritala, J. Mater. Chem. **17**, 5077 (2007).

[22]T. Pilvi, E. Puukilainen, K. Arstila, M. Leskelä, and M. Ritala, Chem. Vapor Depos. **14**, 85 (2008).

[23]T. Pilvi, E. Puukilainen, U. Kreissig, M. Leskelä, and M. Ritala, Chem. Mater. **20**, 5023 (2008).

[24]T. Pilvi, E. Puukilainen, F. Munnik, M. Leskelä, and M. Ritala, Chem. Vapor Depos. **15**, 27 (2009).

[25]M. Mäntymäki, M. J. Heikkilä, E. Puukilainen, K. Mizohata, B. Marchand, J. Räisänen, M. Ritala, and M. Leskelä, Chem. Mater. **27**, 604 (2015).

[26]M. Mäntymäki, K. Mizohata, M. J. Heikkilä, J. Räisänen, M. Ritala, and M. Leskelä, Thin Solid Films **636**, 26 (2017).

[27] PA. Hansen, T. Zikmund, T. Yu, J. Nitsche Kvalvik, T. Aarholt, Ø. Prytz, A. Meijerink, and O. Nilsen, Commun. Chem. **3**, 162 (2020).

[28]M. Mäntymäki, J. Hämäläinen, E. Puukilainen, F. Munnik, M. Ritala, and M. Leskelä, Chem. Vapor Depos. **19**, 111 (2013).

[29]PDF 37–1487, JCPDS-ICDD, International Center for Diffraction Data.

[30]S. Sato, R. Takahashi, M. Kobune, and H. Gotoh, Appl. Catal. A-Gen. **356**, 57 (2009).

[31]PDF 23–1418, JCPDS-ICDD, International Center for Diffraction Data.

[32]https://www.americanelements.com/terbium-fluoride-13708-63-9, visited September 17, 2020.

[33]M. Mäntymäki, J. Hämäläinen, E. Puukilainen, T. Sajavaara, M. Ritala, and M. Leskelä, Chem. Mater. **25**, 1656 (2013).

[34]R. D. Shannon, R. C. Shannon, O. Medenbach, and R. X. Fischer, J. Phys. Chem. Ref. Data **31**, 931 (2002).

[35]I. H. Malitson, J. Opt. Soc. Am. **52**, 1377 (1962).